Submitted to Phys. Plasmas, Nov. 15, 1996

Gyrofluid simulations of turbulence suppression in reversed-shear experiments on the Tokamak Fusion Test Reactor

M. A. Beer, G. W. Hammett, G. Rewoldt, E. J. Synakowski, M. C. Zarnstorff, and W. Dorland[1]

Princeton University Plasma Physics Laboratory, Princeton, NJ 08543
[1]Institute for Fusion Studies, Austin, TX 78712-1060

Abstract

The confinement improvement in reversed-shear experiments on the Tokamak Fusion Test Reactor [Plasma Phys. Controlled Fusion **26**, 11 (1984)] is investigated using nonlinear gyrofluid simulations including a bounce-averaged trapped electron fluid model. This model includes important kinetic effects for both ions and electrons, and agrees well with linear kinetic theory. Both reversed shear and the Shafranov shift reverse the precession drifts of a large fraction of the trapped electrons, which significantly reduces the growth rate of the trapped electron mode, found to be the dominant instability in the core. Two positive feedback transition mechanisms for the sudden improvement in core confinement are discussed: (1) Shafranov shift suppression of the trapped electron mode, and (2) turbulence suppression by radially sheared $\mathbf{E} \times \mathbf{B}$ flows. While both effects appear to be playing roles in the transition dynamics in most experiments, we show that Shafranov shift stabilization alone can cause a transition.

PACS numbers: 52.65.Tt, 52.35.Qz, 52.55.Fa, 52.35.Ra

I. Introduction

In this paper, we investigate the improved confinement with reversed magnetic shear[1,2] using nonlinear gyrofluid simulations extended to higher accuracy[3] and including a bounce-averaged trapped electron fluid model.[4] This nonlinear electron fluid model includes the kinetic effects of the trapped-electron precession resonance and retains the full pitch angle dependence of the electron response. Retaining the pitch angle dependence is essential to describe the suppression of Trapped Electron Modes (TEM) in Enhanced Reversed Shear (ERS) discharges where the dominant stabilizing effect is the reversal of the toroidal precession drifts of barely trapped electrons. This model has been validated by detailed linear comparisons with the most comprehensive kinetic calculations,[5–7] and has extended our simulations to include the ERS and supershot core in the Tokamak Fusion Test Reactor (TFTR),[8] where the dominant instability is the TEM. In the core of RS plasmas (before the transition to ERS) and supershots, our simulations predict fluxes in rough agreement with TRANSP,[9] and the ion heat transport is convection dominated. After the transition to ERS, the TEM is strongly suppressed by the combination of negative magnetic shear and the Shafranov shift. In ERS, the Shafranov shift becomes very large, and is more important than negative magnetic shear in reversing the drifts of the trapped electrons. After the transition, a shorter wavelength TEM is still weakly unstable, but nonlinear simulations find that the transport is reduced by about a factor of 40, in rough agreement with experiment, although the electron heat transport is underestimated. In contrast to magnetic shear, the Shafranov shift stabilization is a positive feedback mechanism and is a possible trigger for the sudden transition to ERS, since steeper pressure gradients lead to larger shifts, more drift reversal, less transport, and in turn, to even steeper pressure gradients. Another potentially important mechanism is stabilization via radially sheared electric fields.[10–13] We find that in ERS, the amount of electric field shear is usually near the level required to completely stabilize the TEM, but that without the Shafranov shift stabilization, the growth rates are too high for the measured levels of $\mathbf{E}\times\mathbf{B}$ shear to stabilize the turbulence. Therefore, both stabilization mechanisms seem to be important in causing the transition. Further studies are needed to elucidate the relative importance of these two mechanisms.

II. Basic model and linear results

To accurately describe the core confinement improvement in ERS discharges, kinetic effects are crucial. Our basic model consists of six-moment toroidal ion gyrofluid equations[3] for each ion species (typically D, C, and a Maxwellian beam component), and bounce-averaged fluid equations for the trapped electrons,[4] coupled by quasineutrality. These equations employ the electrostatic approximation, which is supported by previous results[6,7] showing that the dominant finite-β effect comes through variations in the magnetohydrodynamic (MHD) equilibrium, and the effects of coupling to magnetic fluctuations are much smaller for the β values considered here. The toroidal ion equations include the kinetic effects of parallel[14] and toroidal drift phase mixing, Finite Larmor Radius (FLR) effects,[15] and trapped ion effects. The electron equations include toroidal precession drift phase mixing, and because the electron moments are functions of pitch angle, we use a pitch angle scattering operator for electron-electron and electron-ion collisions.[4] With

this collision operator, the electron equations are continuously valid from the collisionless regime, where the non-adiabatic electron response is driven by the trapped electron precession resonance, to the plateau collisional regime where the electrons become adiabatic. These equations have been carefully benchmarked against linear kinetic theory. Figure 1 shows a comparison of the linear growth rate from this model with fully kinetic calculations[5] for the parameters $\eta_e = \eta_i = 3$, $L_n/R = 1/3$, $\varepsilon = 1/6$, $\hat{s} = 1$, $q = 1.5$, and $\beta = 0$, as the collisionality is varied, demonstrating good agreement.

We now examine the linear instabilities in an ERS mode. Figure 2 shows linear growth rates and real frequencies vs. minor radius well after the transition to ERS. The measured experimental parameters at each radius (from TRANSP) are used as inputs for the calculations. The eigenfrequencies shown are for the fastest growing mode, with γ maximized over $k_\theta \rho_i$. In the core region, $r/a < 0.45$, the dominant instability is a high-k_θ trapped electron mode, and a lower k_θ Ion Temperature Gradient (ITG) driven mode is dominant for $r/a > 0.45$. When the trapped electrons are turned off by assuming an adiabatic electron response, the measured profiles are stable for $r/a < 0.45$. This behavior is typical of RS modes, ERS modes and supershots: the TEM is the dominant instability in the core region where the density gradients are steep, outside this region the ITG mode dominates, and also in L-modes. Both the kinetic and gyrofluid calculations use general magnetic geometry, but the kinetic calculation uses a slowing-down beam distribution function while the gyrofluid calculation uses a Maxwellian beam distribution. The ITG mode is stable in the core because of the steep ∇n_i and low η_i. Although the TEM in the core has a larger peak growth rate, it causes much less transport than the ITG mode which is unstable for $r/a > 0.45$, since the ITG mode is unstable at significantly longer wavelengths. Across the transition from RS to ERS, the longest wavelength trapped electron modes are stabilized, reducing the transport.

III. Finite-β Stabilization of the trapped electron mode

We now discuss the physical mechanisms which stabilize the trapped electron mode in the core. Both negative magnetic shear and the Shafranov shift cause favorable precession of all but deeply trapped electrons and can stabilize the TEM. The precession reversal due to negative $\hat{s}$ is relatively well known, and its stabilizing influence has been thoroughly discussed recently.[16] The finite-β drift reversal effect was first pointed out in Ref. 17. We begin by using the $\hat{s} - \alpha$ model equilibrium to demonstrate this effect, where the Shafranov shift effects are measured by $\alpha = -q^2 R d\beta/dr$. The precession drift is the the bounce-average of the ∇B and curvature drifts, and in the $\hat{s} - \alpha$ model is given by:

$$\langle \omega_{de} \rangle_b(\kappa) = \frac{k_\theta \rho_e v_{te}}{R} \langle \cos\theta + (\hat{s}\theta - \alpha \sin\theta) \sin\theta \rangle_b \tag{1}$$

$$= \frac{k_\theta \rho_e v_{te}}{R} [G_0(\kappa) + \hat{s} G_s(\kappa) + \alpha G_\alpha(\kappa)]$$

where $G_0(\kappa) = 2E(\kappa^2)/K(\kappa^2) - 1$, $G_s(\kappa) = 4[E(\kappa^2)/K(\kappa^2) + \kappa^2 - 1]$, and $G_\alpha(\kappa) = (4/3)[(1-2\kappa^2)E(\kappa^2)/K(\kappa^2) + \kappa^2 - 1]$, where E and K are complete elliptic integrals, and κ is a pitch angle variable which is zero for deeply trapped electrons and one for barely trapped electrons, as defined in Ref. 4. Figure 3 shows these three terms.

Since $G_s > 0$ and $G_\alpha < 0$, both negative $\hat{s}$ and positive α reverse the precession of barely trapped electrons. This drift reversal is stabilizing, as the reversed electrons can no longer resonate with the TEM.

For TFTR ERS core parameters, the Shafranov shift induced drift reversal (α) actually dominates, since the shear is only weakly negative, $\hat{s} \sim -1/4$, but the shift becomes very large, $\alpha \sim 2$, typical parameters of the second stability regime to MHD ballooning modes. We show this in Fig. 4 by varying $\hat{s}$ and α, keeping other parameters fixed, for $r/a = 0.25$ at $t = 3$s of TFTR shot 84011. Using $\hat{s} = 0.25$ and $\alpha = 0.3$, values typical of the supershot regime, very few electrons have reversed precession, as shown in Fig. 4(a). The corresponding growth rates for the trapped electron mode are shown in Fig. 4(b). Reversing the magnetic shear to values typical in the reversed shear mode before the transition (RS), $\hat{s} = -0.25$, but before the shift has become large, $\alpha = 0.3$, reverses the precession drifts of more of the barely trapped electrons and stabilizes the TEM somewhat. Using the measured parameters after the transition, $\hat{s} = -0.25$ and $\alpha = 2.5$, we find much more drift reversal. The long wavelengths are stabilized, and the remaining high-k TEM is quite weak and causes little transport. Thus, the effect on the growth rates of reversed shear alone is rather weak, but the combined effects of reversed shear and the Shafranov shift are very strongly stabilizing.

To more accurately describe this effect, we have extended our simulations to general magnetic geometry. Using the output of an equilibrium code, we numerically compute the dependence along the field line coordinate, θ, of the geometric terms which enter the gyrofluid equations, as described in Ref. 18: $\omega_d(\theta)$, $k_\perp(\theta)$, $\hat{\mathbf{b}} \cdot \nabla(\theta)$, and $B(\theta)$. In addition, we numerically bounce average $\omega_d(\theta)$ to calculate the toroidal precession frequency for the trapped electrons: $\langle \omega_d \rangle_b (\kappa)$. To show the effects of full geometry on the precession frequency, we calculate equilibria using JSOLVER[19] and the measured TFTR profiles after the transition, at $t = 3.0$s. We can also artificially reduce the Shafranov shift, by repeating the equilibrium calculation with all densities reduced by a factor of 10. We then numerically calculate the bounce averaged curvature and ∇B drifts using the JSOLVER output. The toroidal precession frequencies are compared for these two cases in Fig. 5. Because the q profile changes slightly when the density is reduced, we compare at $r/a = 0.3$, where $\hat{s} = -.17$ and $\Delta' = .53$ for the full density case ($\Delta' = d\Delta/dr$, where Δ is the Shafranov shift), and at $r/a = 0.26$ for the reduced density case where the shear is the same, $\hat{s} = -.17$, and $\Delta' = .07$. The effect of the Shafranov shift is quite striking, and is significantly different from that given by the $\hat{s} - \alpha$ model, though the basic trend is similar. Because of the pitch-angle (κ) dependence of the Jacobian of the transformation to v, κ variables, the fraction of electrons with drift reversal is given by $n_e/n_{e0} = 1 - \int_{-\theta_t}^{\theta_t} (d\theta/4) \sqrt{1 - (B/B_{\min})(1 - 2\varepsilon_B \kappa_0^2)}$, where $\langle \omega_{de} \rangle_b (\kappa_0) = 0$, θ_t is the turning point for a particle with $\kappa = \kappa_0$, and other notation is defined in Ref. 4. From Fig. 5, we find 75% drift reversal at $\Delta' = .53$ and 60% drift reversal at $\Delta' = .07$. We have also calculated the case with $\Delta' = .07$ and $\hat{s} = 0$, at $r/a = .29$, and find 40% drift reversal.

Some of the differences between the full geometry results and the $\hat{s} - \alpha$ model can be understood by looking at the precession drift frequency in the low-β, small $\varepsilon = r/R$ limit, where $\beta \sim O(\varepsilon^2)$ and $\Delta' \sim O(\varepsilon)$. The combined curvature and ∇B drift frequency is (for $\theta_0 = 0$):

$$i\omega_d \Phi \propto \frac{v_{te}^2}{2\Omega_e B^2} [\mathbf{B} \times \nabla B + B^2 \hat{\mathbf{b}} \times (\hat{\mathbf{b}} \cdot \nabla \hat{\mathbf{b}})] \cdot \nabla \Phi, \tag{2}$$

and for low β and small ε, this becomes:

$$\omega_d \approx \cos\theta - (\Delta' + \varepsilon) + \frac{\varepsilon}{q^2} + \hat{s}\theta\sin\theta - r\Delta''\sin^2\theta \tag{3}$$

$$+\Delta'\hat{s}\theta\sin\theta\cos\theta - \hat{s}\sin^2\theta\left(\Delta' + \varepsilon\right) + O(\varepsilon^2).$$

Comparison with Eq. (1) shows that the $\hat{s}-\alpha$ model only keeps three of these terms, the $\cos\theta$ term, the $\hat{s}\theta\sin\theta$ term, and the $-r\Delta''\sin^2\theta$ term, which corresponds to the $\alpha\sin^2\theta$ term in Eq. (1), because $\Delta' \propto (l_i/2+\beta_\theta)\,r$ and $\alpha = -q^2R(d\beta/dr) \propto \Delta''$. The $\hat{s}-\alpha$ model misses the reduction in precession frequency for all particles (not just the deeply trapped particles) from Δ'. This Δ' reduction of ω_d arises from compression of the flux surfaces and a change in the tilt of the field lines, which comes from variations in B_p over the surface. This reduces k_θ in the bad curvature region and increases k_θ in the good curvature region, in addition to a $\sin\theta$ variation in k_r proportional to Δ'. These pieces combine with the $\hat{\theta}\cos\theta + \hat{\mathbf{r}}\sin\theta$ variation of $\mathbf{B}\times\nabla B$ to give the constant Δ' reduction in $\omega_d(\theta)$, which after bounce averaging leads to a constant Δ' reduction in $\langle\omega_d\rangle_b(\kappa)$, independent of pitch angle. In this ordering, $\beta \sim O(\varepsilon^2)$, which is reasonably well satisfied for TFTR, the changes in B are subdominant. The Shafranov shift also reduces the field line length in the bad curvature region and increases the field line length in the good curvature region, but this does not affect the constant Δ' reduction in $\langle\omega_d\rangle_b$, since the bounce averaged drift $\langle\omega_d\rangle_b = (\oint dl\,\omega_d/|v_{||}|)/(\oint dl/|v_{||}|)$. Using $dl = (rB/B_p)\,d\theta \approx qR_0(1-\Delta'\cos\theta)\,d\theta$, we find $\tau_b = \oint dl/|v_{||}| \propto [1-(\Delta'-\varepsilon/2)G_0]K(\kappa^2)$, and

$$\langle\omega_d\rangle_b = G_0 - (\Delta'+\varepsilon) + \frac{\varepsilon}{q^2} + (\Delta' - \frac{\varepsilon}{2})(G_0^2 - 1 - G_\alpha) + \hat{s}G_s(1 + \Delta' G_0 - \frac{\varepsilon}{2}G_0) \tag{4}$$

$$+(r\Delta'' + \hat{s}\Delta' + \hat{s}\varepsilon)G_\alpha + \frac{\hat{s}\varepsilon}{6}\left(2G_s(1-2\kappa^2) - G_\alpha\right) + O(\varepsilon^2),$$

where the G's are defined following Eq. (1) and are plotted in Fig. 3. The unusual feature of Shafranov shift stabilization of the TEM is that it becomes more stabilizing for steeper pressure gradients, and allows access to what could appropriately be called the second stability regime to the TEM. This feature also makes Shafranov shift stabilization a potential positive feedback mechanism to produce the sudden transition to improved confinement in ERS.

IV. ERS transition mechanisms

To get a sudden transition or bifurcation to the improved confinement in ERS, transport must decrease as the driving gradients are increased, providing the positive feedback necessary for the core density to run away. There appear to be two potential mechanisms which can produce this positive feedback:

1. The stabilization of the TEM from the Shafranov shift,[20] and
2. Radial $\mathbf{E}\times\mathbf{B}$ flow shear stabilization of the turbulence.[10]

As discussed below, it appears that both of these effects may produce a transition individually, or in tandem. Both of these effects are stronger in ERS plasmas than in other tokamak regimes. ERS modes have unusually

large Δ' since both q and β are large in core, so Shafranov shift stabilization is enhanced. This becomes a positive feedback mechanism when the Shafranov shift stabilization is strong enough to overcome the increased instability drive from the steeper gradients. Then as ∇p increases, Δ' increases, the transport decreases, and the pressure gradients steepen further.

When the shearing rate, ω_E, from radial $\mathbf{E}\times\mathbf{B}$ flow shear is on the order of or larger than the maximum linear growth rate, $\omega_E > \gamma$, the turbulence can be completely stabilized.[12] When the radial electric field is driven by the pressure gradient, this is also a positive feedback mechanism, since as ∇p increases, E_r' increases, the transport decreases, and the pressure gradients steepen further. This effect is also strong in the ERS regime, since ERS modes have large ∇p. The appropriate shearing rate in general geometry[11] is $\omega_E = (RB_p/B)d/dr(E_r/B_pR)$, and since B_p is small in the core of ERS modes, the shearing rate is enhanced. In addition, the Shafranov shift enhances ω_E. Turbulence suppression by radial $\mathbf{E}\times\mathbf{B}$ flow shear has been shown to be consistent with the transition to improved confinement in ERS in Ref. 21.

Figure 6 compares the measured $\mathbf{E}\times\mathbf{B}$ shearing rate within the good confinement zone, at $r = .25a$, to the maximum linear growth rate calculated at the same radius, for an ERS mode which transitioned at $t = 2.71$s. The measured $\mathbf{E}\times\mathbf{B}$ shearing rate is larger than γ after the transition, demonstrating that ω_E is large enough to substantially suppress the turbulence. Also shown are the linear growth rates without Shafranov shift stabilization ($\Delta' = 0$), where the linear growth rates are too large for ω_E to completely stabilize the turbulence. Therefore, in this case it appears that both mechanisms are playing a role: Shafranov shift stabilization keeps the linear growth rates from increasing with the pressure gradient, and eventually ω_E overcomes $\gamma_{\rm lin}$. It is difficult to perform experiments which clearly separate these two effects, since both are proportional to ∇p, and both Δ' and E_r' usually increase dramatically across the transition. Back-transition experiments on TFTR[22] varying the co-counter beam fraction indicate that decreasing E_r' can cause the plasma to drop out of ERS, indicating that E_r' is playing a key role in maintaining the transport barrier. There are cases, however, where the criterion $\omega_E > \gamma$ does not correlate well with the transition.[23] The observed B scaling of the threshold power, $\propto B^2$, also seems more consistent with a transition induced by Shafranov shift stabilization, since $\Delta' \propto \beta$.

We now describe a theoretical experiment which shows that the Shafranov shift appears to be able to produce a transition independently, without ω_E stabilization. To cause a transition, Shafranov shift stabilization must overcome the increased transport from steeper gradients. To test this effect, we generate a series of equilibia using JSOLVER,[19] starting with the measured profiles at $t = 3$s, and gradually decreasing all densities. This gives a series of equilibria with $\Delta' \propto n$, and very similar q profiles. We then calculate the particle flux, $\Gamma = -D\nabla n$, for each of these equilibria, either by using fully nonlinear simulations or by estimating the particle diffusivity D from the maximum over k_θ of $\gamma/k_\perp^2$, which correlates well with our nonlinear simulations.[24] The results are shown in Fig. 7, using $D = (5/3)\gamma/k_\perp^2$ from linear calculations with the $\hat{s}-\alpha$ model and with full geometry, and two nonlinear simulations in full geometry. The two nonlinear simulations agree well with the $\gamma/k_\perp^2$ estimate with a proportionality constant of $5/3$. Fig. 7(a) is within the good confinement zone, at $r/a = 0.3$. At small density gradients, we find the usual situation where steeper density gradients cause more transport. But at roughly 60% of the measured density gradient at $t = 3$s,

the stabilization from the Shafranov shift overcomes the increasing density gradient and causes a transition, since beyond this point steeper densities cause less transport and the density runs away. Fig. 7 shows the same calculation, at $r/a = 0.5$, outside the good confinement zone. Here, transport continues to increase with increasing density, so no runaway occurs. Thus, this result correlates well with the observed transport barrier location in the experiment.

In the experiments, however, the entire density profiles do not increase; the density only increases in the core. We thus repeat the above experiment only changing the density in the good confinement zone, out to the "knee" in the density profile at $r/a = .45$. This series also decreases $L_n = (\frac{1}{n_0}\frac{dn_0}{dr})^{-1}$, and increases the instability drive at the same time that Δ' is increased. These results are shown in Fig. 8. The Shafranov shift still overcomes the increased drive and causes a transition at about half the measured gradient. In Fig. 8 we have also schematically indicated the effects of ω_E, which are not included in these calculations, by reducing the flux by a contribution proportional to $\nabla n/(1-\Delta')^2$, including the Shafranov shift enhancement of ω_E. Since $\mathbf{E}\times\mathbf{B}$ shear is also $\propto \nabla n$, the stabilization from ω_E increases with ∇n, and reduces the threshold gradient by shifting the peak of the flux vs. ∇n curve to lower ∇n.

V. Nonlinear Simulations

We now describe nonlinear toroidal gyrofluid simulation results, including deuterium, carbon, and trapped electrons for an ERS discharge within the good confinement zone, at $r/a = .25$, where the turbulence is driven by trapped electron modes. The results just before the transition, at $t = 2.66$s, are shown in Fig. 9(a). We find reasonable agreement with measured fluxes: the predicted fluxes are about three times the measured values from TRANSP. In addition, the ion heat flux is convection dominated, as seen experimentally. A simulation using measured input parameters after the transition is shown in Fig. 9(b). The turbulent fluxes drop by about a factor of 40 compared to the pre-transition simulation, and the fluctuation levels drop dramatically. However, this run has not yet reached a satisfactory steady state, which would require a much longer run with these small growth rates. Another caveat is that so close to marginal stability, the simulation results are very sensitive to input gradients. Although the electron heat flux is below experimental measurements after the transition, the dramatic confinement improvement across the transition is reproduced.

VI. Conclusions and Discussion

To summarize, we have investigated the confinement improvement in ERS regimes using nonlinear gyrofluid simulations. Our comprehensive gyrofluid model[3,4] agrees with kinetic calculations, where we find that a high-k_θ trapped electron mode is the dominant instability in the steep density gradient core region, and that a lower-k_θ ITG mode is unstable for $r/a > 0.45$. Our pitch angle dependent trapped electron model was required to capture precession drift reversal, which greatly reduces the growth rate of the TEM in the core. The Shafranov shift accounts for much of this drift reversal, and we have extended our simulations to general geometry to accurately capture this effect. Shafranov shift stabilization is also a potential positive feedback

mechanism to produce the sudden transition to enhanced confinement in ERS. We also show that turbulence suppression via radial electric field shear is often important, and usually find $\gamma_{\rm lin} \sim \omega_E$ at the transition. It appears that both effects are working together to produce the transition: Shafranov shift stabilization keeps the growth rates from increasing with the driving gradients, and keeps the turbulence weak enough to allow the increasing pressure driven $\mathbf{E} \times \mathbf{B}$ shear to further stabilize the turbulence. Finally, our nonlinear simulations capture the main features of the transition to ERS, even though they do not include equilibrium scale sheared $\mathbf{E} \times \mathbf{B}$ flows. The calculated pre-transition fluxes are in rough agreement with TRANSP, the core ion heat transport mostly convective, and we find a sharp drop in transport at transition, as the long wavelengths are stabilized, and the remaining high-k TEM causes little transport.

Many questions for future work remain. Perhaps some high-k mode or subcritical c/ω_{pe} scale turbulence is causing the residual electron transport after the large scale turbulence is stabilized. We plan to include E_r' in our nonlinear gyrofluid simulations to investigate parametric dependences of the approximate criterion $\gamma_{\rm lin} \sim \omega_E$. A crucial question for future experiments is whether we can find a regime where Shafranov shift stabilization alone gives turbulence suppression. The Shafranov shift has a more favorable scaling to reactors than E_r', since the Shafranov shift is independent of machine size, while E_r' effects become weaker in larger machines. An exciting alternative is to drive E_r' with Ion Bernstein Waves instead of pressure or velocity gradients. We are also beginning to investigate other geometries which may more transition more easily. Oblate reversed triangularity[25] tokamaks, which have stronger Shafranov shifts at the same β as conventional tokamaks, are one possibility. Low aspect ratio tokamaks, such as the proposed National Spherical Torus eXperiment, have naturally large drift reversal from low R/a and high Δ', and Shafranov shift stabilization should be quite strong. Finally, perhaps stellarator configurations can be optimized for drift reversal to take advantage of the confinement improvement in ERS. Our results indicate that obtaining steep density gradients may be crucial, since it appears to be easier to stabilize the TEM (through the Shafranov shift and precession drift reversal) than the ITG mode.

Acknowledgements

This work was supported in part by an appointment to the U. S. Department of Energy Fusion Energy Postdoctoral Research Program administered by the Oak Ridge Institute for Science and Education and in part by U.S. DOE Contract No. DE-AC02-76CHO3073. M.A.B. would like to thank Dr. M. Kotschenreuther for useful discussions, help implementing general geometry, and linear benchmarking, Dr. R. White for useful discussions on geometry, and Dr. J. Manickam for providing the equilibrium code. This work contributes to the Numerical Tokamak Turbulence Project Grand Challenge Application, which is supported jointly by the U.S. DOE Office of Fusion Energy Sciences and the Mathematics, Information, and Computational Sciences Division as part of the High Performance Computing and Communications Program.

References

[1]F. M. Levinton, M. C. Zarnstorff, S. H. Batha, M. Bell, R. E. Bell, R. V. Budny, C. Bush, Z. Chang, E. Fredrickson, A. Janos, J. Manickam, A. Ramsey, S. A. Sabbagh, G. L. Schmidt, E. J. Synakowski, and G. Taylor, Phys. Rev. Lett. **75**, 4417 (1995).

[2]E. J. Strait, L. L. Lao, M. E. Mauel, B. W. Rice, T. S. Taylor, K. H. Burrell, M. S. Chu, E. A. Lazarus, T. H. Osborne, S. J. Thompson, and A. D. Turnbull, Phys. Rev. Lett. **75**, 4421 (1995).

[3]M. A. Beer and G. W. Hammett, Phys. Plasmas **3**, 4046 (1996).

[4]M. A. Beer and G. W. Hammett, Phys. Plasmas **3**, 4018 (1996).

[5]M. Kotschenreuther, G. Rewoldt, and W. M. Tang, Comp. Phys. Commun. **88**, 128 (1995).

[6]G. Rewoldt, W. M. Tang, and M. S. Chance, Phys. Fluids **25** 480 (1982).

[7]G. Rewoldt, W. M. Tang, and R. J. Hastie, Phys. Fluids **30** 807 (1987).

[8]K. M. Young, Plasma Phys. Controlled Fusion **26** 11, (1984).

[9]R. J. Hawryluk, in *Physics of Plasmas Close to Thermonuclear Conditions* (Commission of the European Communities, Brussels, 1980), Vol. 1, p. 19.

[10]P. H. Diamond, V. B. Lebedev, D. E. Newman, B. A. Carreras, T. S. Hahm, W. M. Tang, G. Rewoldt, and K. Avinash, *On the transition to enhanced confinement in reversed magnetic shear discharges,* submitted to Phys. Rev. Lett.; V. B. Lebedev, P. H. Diamond, M. B. Isichenko, P. N. Yushmanov, D. E. Newman, B. A. Carreras, V. E. Lynch, T. S. Hahm, W. M. Tang, G. Rewoldt, K. Avinash, and A. Smolyakov, in *Proceedings of the 16th International Conference on Plasma Physics and Controlled Nuclear Fusion Research, 1996* (International Atomic Energy Agency, Vienna) paper IAEA-CN-64/D1-3; see also R. E. Waltz, G. M. Staebler, G. W. Hammett, and J. A. Konings, in *Proceedings of the 16th International Conference on Plasma Physics and Controlled Nuclear Fusion Research, 1996* (International Atomic Energy Agency, Vienna) paper IAEA-CN-64/D1-6.

[11]T. S. Hahm and K. H. Burrell, Phys. Plasmas **2**, 1648 (1995).

[12]R. E. Waltz, G. D. Kerbel, and J. Milovich, Phys. Plasmas **1**, 2229 (1994).

[13]M. Artun, W. M. Tang, and G. Rewoldt, Phys. Plasmas **2**, 3384 (1995)

[14]G. W. Hammett and F. W. Perkins, Phys. Rev. Lett. **64**, 3019 (1990).

[15]W. Dorland and G. W. Hammett, Phys. Fluids B **5**, 812 (1993).

[16]C. Kessel, J. Manickam, G. Rewoldt, and W. M. Tang, Phys. Rev. Lett. **72**, 1212 (1994).

[17]M. N. Rosenbluth and M. L. Sloan, Phys. Fluids **14**, 1725 (1971).

[18]M. A. Beer, S. C. Cowley, and G. W. Hammett, Phys. Plasmas **2**, 2687 (1995).

[19]J. DeLucia, S. C. Jardin, and A. M. M. Todd, J. Comp. Phys. **37**, 183 (1980).

[20]M. A. Beer and G. W. Hammett, Bull. Am. Phys. Soc. **40**, 1733 (1995).

[21]E. Mazzucato, S. H. Batha, M. Beer, M. Bell, R. E. Bell, R. V. Budny, C. Bush, T. S. Hahm, G. W. Hammett, F. M. Levinton, R. Nazikian, H. Park, G. Rewoldt, G. L. Schmidt, E. J. Synakowski, W. M. Tang, G. Taylor, and M. C. Zarnstorff, Phys. Rev. Lett. **77**, 3145 (1996).

[22]E. J. Synakowski, S. Batha, M. A. Beer, M. G. Bell, R. E. Bell, R. V. Budny, C. E. Bush, P. C. Efthimion, G. W. Hammett, T. S. Hahm, B. LeBlanc, F. M. Levinton, E. Mazzucato, H. Park, A. T. Ramsey, G. Rewoldt, S. D. Scott, G. Schmidt, W. M. Tang, G. Taylor, and M. C. Zarnstorff, *The roles of electric field shear and Shafranov shift in sustaining high confinement in enhanced reversed shear plasmas on the TFTR tokamak*, submitted to Phys. Rev. Lett. Also see E. J. Synakowski, S. Batha, M. A. Beer, M. G. Bell, R. E. Bell, R. V. Budny, C. E. Bush, P. C. Efthimion, G. W. Hammett, T. S. Hahm, B. LeBlanc, F. M. Levinton, E. Mazzucato, H. Park, A. T. Ramsey, G. Rewoldt, S. D. Scott, G. Schmidt, W. M. Tang, G. Taylor, and M. C. Zarnstorff, Phys. Plasmas, this issue.

[23]M. C. Zarnstorff, M. A. Beer, F. M. Levinton, S. D. Scott, E. J. Synakowski, and the TFTR team, Bull. Am. Phys. Soc. **41**, 1447 (1996).

[24]M. Kotschenreuther, W. Dorland, M. A. Beer, and G. W. Hammett, Phys. Plasmas **2**, 2381 (1995).

[25]M. Kotschenreuther, W. Dorland, Q. P. Liu, G. W. Hammett, M. A. Beer, S. A. Smith, A. Bondeson, and S. C. Cowley, in *Proceedings of the 16th International Conference on Plasma Physics and Controlled Nuclear Fusion Research, 1996* (International Atomic Energy Agency, Vienna) paper F1-CN-64/D1-5.

List of Figures

8 Calculated particle flux as ∇n is varied, now only changing the densities within the good confinement zone, $r/a < 0.4$. Again, beyond some critical density gradient, Shafranov shift stabilization of the TEM overcomes the increasing instability drive from the increasing gradient, causing a transition. Including ω_E stabilization would decrease the critical gradient, as shown schematically (dashed line), by shifting the peak of the flux vs. ∇n curve. . . . . .

9 Nonlinear simulations of an ERS discharge at $r/a = 0.25$ (a) before the transition, and (b) after the transition. Before the transition, the predicted fluxes are in reasonable agreement with power balance measurements, and the ion heat flux is convection dominated. After the transition, the transport is greatly reduced, as the longest wavelengths are stabilized by the large Shafranov shift. . . . . .

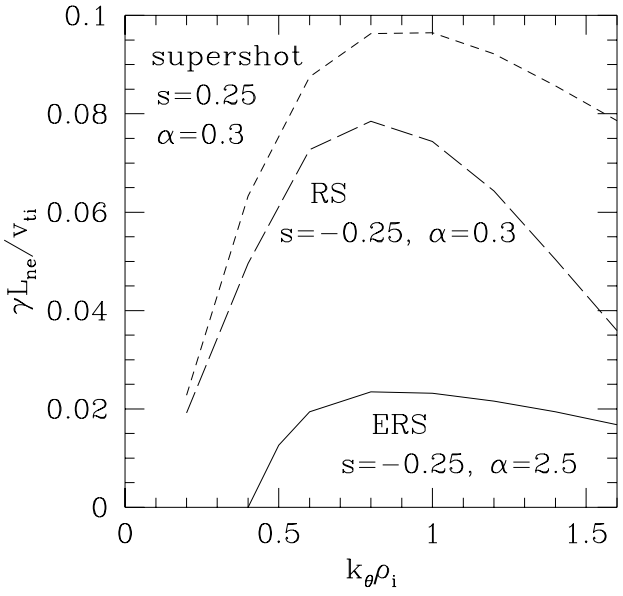
0.1
0.08
0.06
0.04
0.02
0
0
0.5
1
1.5
supershot
s=0.25
α=0.3
RS
s=−0.25, α=0.3
ERS
s=−0.25, α=2.5
γL_ne/v_ti
k_θρ_i

Figure 4(b)

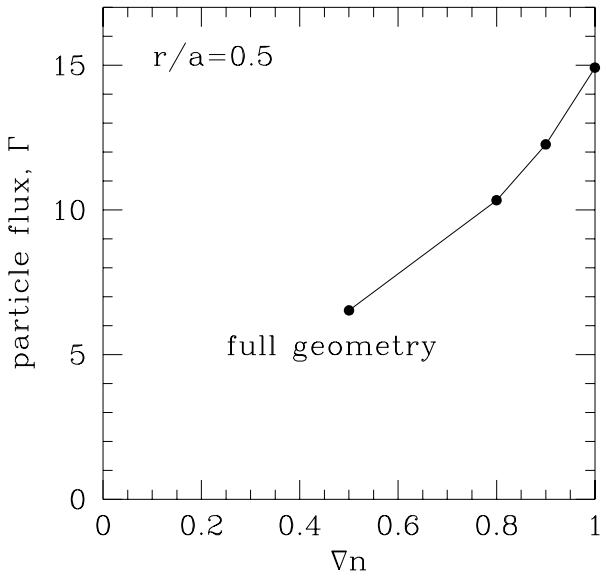

Figure 7(b)

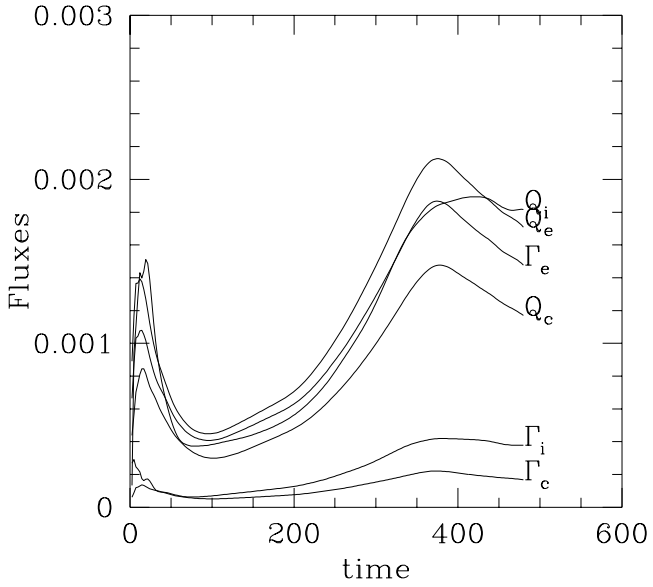
0.003
0.002
0.001
0
Fluxes
0
200
400
600
time
Q_i
Q_e
Γ_e
Q_c
Γ_i
Γ_c

Figure 9(b)

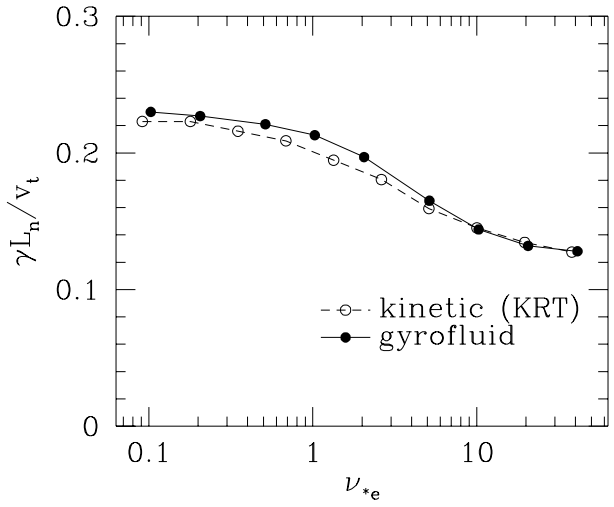

Figure 1:

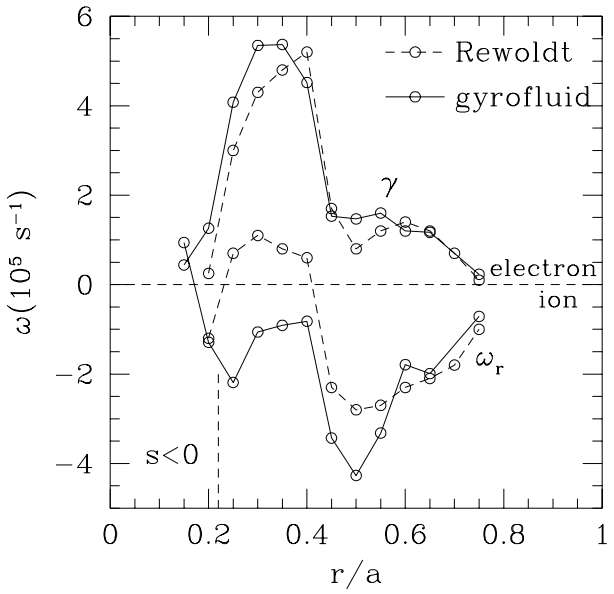
Rewoldt
gyrofluid
γ
electron
ion
ω_r
s<0
ω(10^5 s^-1)
r/a
6
4
2
0
−2
−4
0
0.2
0.4
0.6
0.8
1

Figure 2:

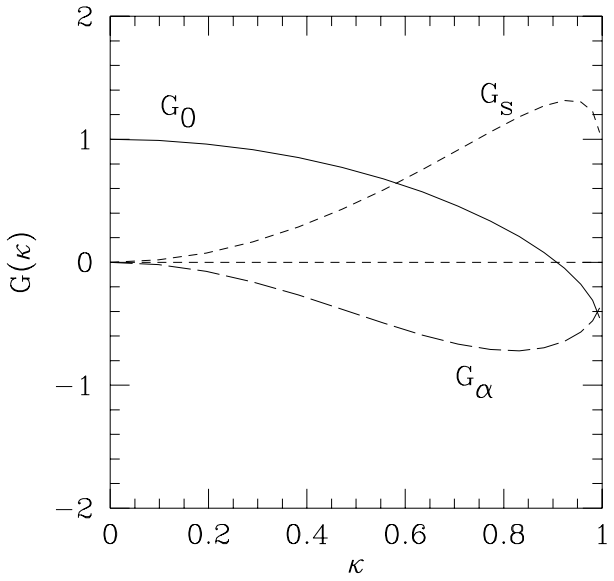

Figure 3:

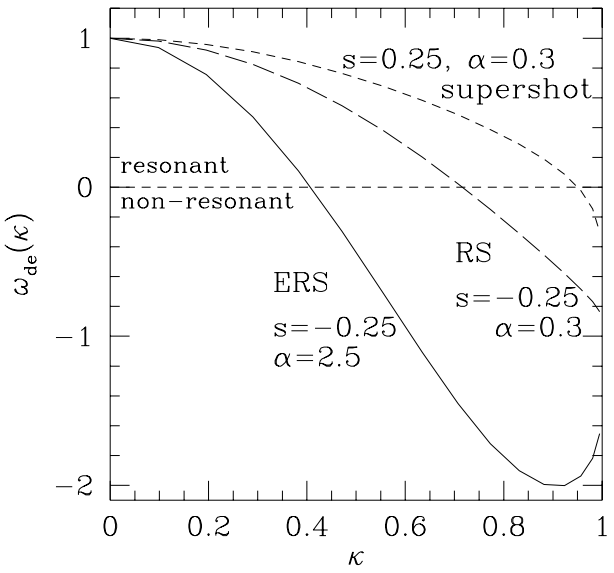
1
0
−1
−2
0
0.2
0.4
0.6
0.8
1
κ
ω_de(κ)
s=0.25, α=0.3
supershot
resonant
non−resonant
RS
s=−0.25
α=0.3
ERS
s=−0.25
α=2.5

Figure 4: (a)

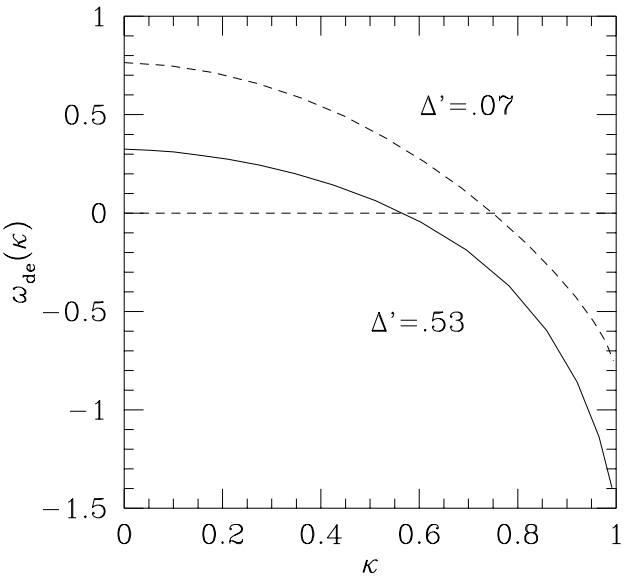

Figure 5:

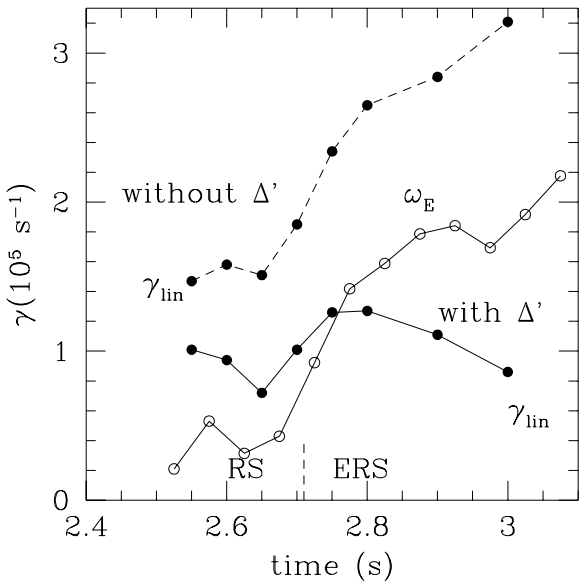
without Δ'
ω_E
γ_{lin}
with Δ'
γ_{lin}
RS
ERS
$\gamma(10^5\ s^{-1})$
time (s)
0
1
2
3
2.4
2.6
2.8
3

Figure 6:

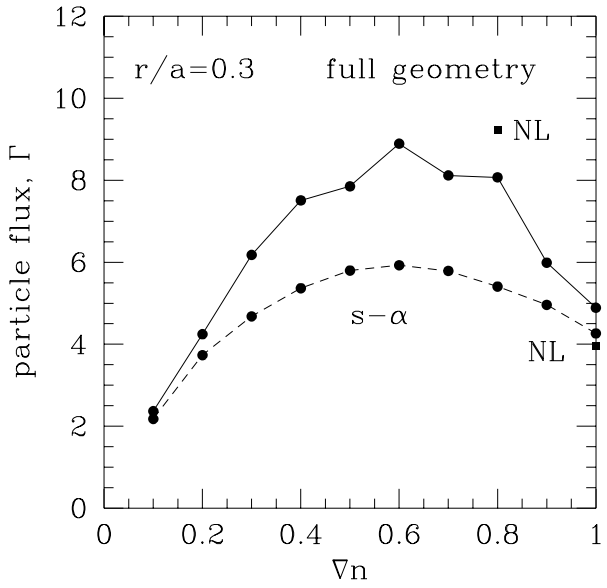
r/a=0.3
full geometry
NL
s−α
NL
particle flux, Γ
∇n
0
2
4
6
8
10
12
0
0.2
0.4
0.6
0.8
1

Figure 7: (a)

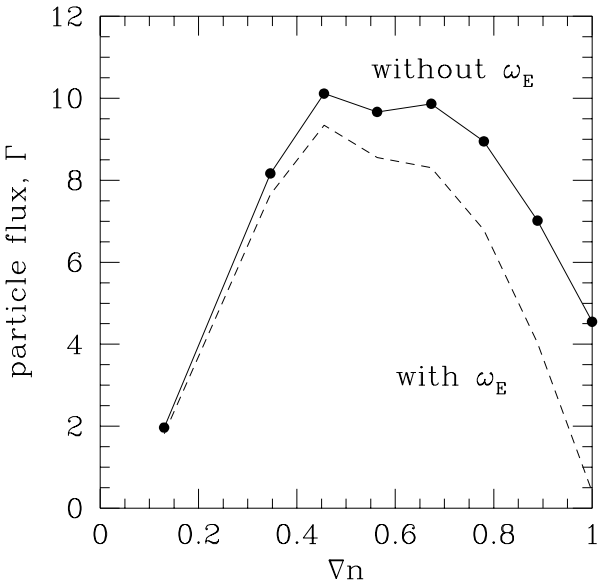

Figure 8:

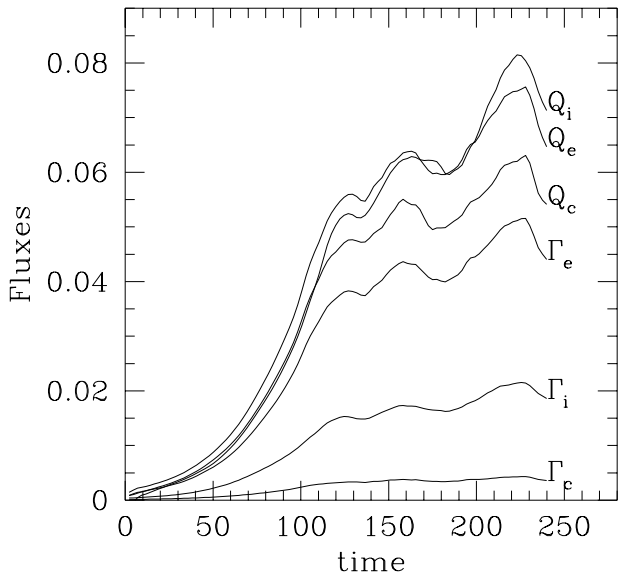
0.08
0.06
0.04
0.02
0
Fluxes
0
50
100
150
200
250
time
Q_i
Q_e
Q_c
Γ_e
Γ_i
Γ_c

Figure 9: (a)